Journal of Electroanalytical Chemistry 1010 (2026) 120044

Contents lists available at ScienceDirect

Journal of Electroanalytical Chemistry

journal homepage: www.elsevier.com/locate/jelechem

Cytochrome b_{562} fusion to formaldehyde dehydrogenase enables increased direct electron transfer

Anna-Lena Drommershausen, Bero H.G. Schnell, Dirk Holtmann *

Process Engineering in Life Sciences 2 – Electro Biotechnology Karlsruhe Institute of Technology, Fritz-Haber-Weg 4, 76131 Karlsruhe, Germany

ARTICLE INFO

Keywords:
Formaldehyde dehydrogenase
Direct electron transfer
Protein engineering
CO_2 reduction
Formaldehyde biosensor
Cofactor-free synthesis

ABSTRACT

Direct electron transfer (DET) between redox enzymes and electrodes is a crucial process in developing biosensors and cofactor-free bio electrosynthesis. However, due to unfavourable orientations, the absence of accessible redox centres, or long electron transfer distances, DET efficiency can be low. Here we present a systematic approach to better understand, evaluate and increase the DET capabilities of a formaldehyde dehydrogenase (F_{ald}DH). F_{ald}DH catalyses the reversible oxidation of formaldehyde to formate and is part of the CO_2 to methanol enzyme cascade. F_{ald}DH from *Burkholderia multivorans* was fused to a DET capable domain, the soluble subunit of cytochrome b_{562} from *Escherichia coli.* Fusion proteins with two different linker morphologies and various lengths were designed and biochemically and electrochemically characterised. The longest flexible linker had minor effects on biochemical constants and exhibited the highest increase in current density. We also identified an undesirable side-reaction between formaldehyde and basic amino acids to interfere with the electrochemical measurements and therefore normalised all currents to the percentage of basic amino acids on the solvent exposed surface area of the protein. This enabled us to present the first protein engineering approach to increase DET in this enzyme, resulting in a 1.6-fold increase in current density, compared to the wild-type enzyme.

1. Introduction

Formaldehyde dehydrogenases (F_{ald}DHs) are zinc-containing enzymes that belong to the medium chain alcohol dehydrogenase/reductase superfamily, which is part of the oxidoreductase enzyme class [1–3]. These enzymes catalyse the NAD^+-dependent oxidation of formaldehyde (FA) to formate (FMT), which can be a cytotoxic by-product of endogenous metabolism [1,4–6]. F_{ald}DHs play an important role in biosensing and enzyme technology. By immobilising F_{ald}DH from *Pseudomonas putida* (*Pp*F_{ald}DH) on gold electrodes it could be shown, that the enzyme can work as a 3rd generation biosensor to detect FA in wastewater [7]. Also, the enzyme is an indispensable part of the multi-enzyme cascade to reduce CO_2 to methanol (Fig. 1) [8]. The biotechnological reduction of CO_2 to methanol is one example of a fossil-free and sustainable process to produce C1-platform chemicals aiming at the establishment of a carbon-neutral bioeconomy. The multi-enzyme cascade was first described in 1999 and till then optimised regarding enzyme concentration and ratio applying various immobilisation techniques [9–13]. However, one major drawback of the cascade is its dependency on NADH as a reduction equivalent. Therefore, researchers have focussed on applying electrochemical principles like mediated electron transfer (MET) and direct electron transfer (DET) to the multi-enzyme cascade [14,15]. Multiple studies have shown that CO_2 can be converted into methanol using DET or MET to regenerate the active site of enzymes, with various electrodes and immobilisation techniques being used. (Fig. 1) [15–18]. This concept of using renewable energy for the conversion of CO_2 to energetic feedstocks, is known as Power-to-X [19]. Recently, the electro-enzymatic cascade could be even further optimised, by immobilising F_{ald}DH and alcohol dehydrogenase (ADH) on a gas-diffusion electrode to directly reduce the electrochemically generated FMT [20].

The underlying principle of DET in enzyme catalysis is cofactor-free synthesis. Hence, the role of the cofactor is replaced by direct electron injection to or from the catalyst, often *via* electrode interactions. DET offers the possibility to run the entire reaction without the need for the costly and challenging to regenerate cofactor NADH [21,22]. However, the principle of DET with F_{ald}DHs is poorly understood and characterised only on the basis of a FA biosensor, hence for the oxidation of FA

* Corresponding author.
E-mail addresses: anna-lena.drommershausen@kit.edu (A.-L. Drommershausen), bero.schnell@kit.edu (B.H.G. Schnell), dirk.holtmann@kit.edu (D. Holtmann).

https://doi.org/10.1016/j.jelechem.2026.120044
Received 18 December 2025; Received in revised form 27 February 2026; Accepted 13 March 2026
Available online 14 March 2026

to FMT [7]. Teišerskytė and coworkers immobilised *Pp*F_{ald}DH on a gold-nanoparticle coated gold electrode and showed that the increase in current density is dependent on the concentration of FA added to the electrochemical cell. We follow this approach and use a FA biosensor to investigate the DET capabilities of a F_{ald}DH derived from *Burkholderia multivorans* (*Bm*F_{ald}DH). *Bm*F_{ald}DH has shown to have a higher activity in the reduction of FMT compared to the *Pp*F_{ald}DH, which is available for purchase [23]. Since not only the cofactor dependency, but also the nature of the FaldDH, as it exhibits weak interactions and a low activity for the reduction reactions, represents a drawback for the CO_2 reduction process, we decided to work with the *Bm*F_{ald}DH. In this study, our aim was to improve the understanding of DET in *Bm*F_{ald}DH, as well as to enhance its DET capabilities through protein engineering. Several studies have summarised different approaches to improving the DET efficiency of enzymes [24,25], like a truncation or deletion of parts of the enzyme [26,27], the application of single point mutations to exhibit electron hopping between aromatic amino acids [28] or the oriented immobilisation of the enzyme on an electrode using fusion tags [29].

In this work, we present the fusion of the *Bm*F_{ald}DH to a DET domain, the soluble part of Cytochrome b_{562} (cyt b_{562}) from *Escherichia coli* (*E. coli*). Approaches have demonstrated, that by fusing the DET domain to a flavin adenine dinucleotide (FAD)-dependent glucose dehydrogenase, it resulted in enhanced DET to electrodes during the glucose oxidation [30]. Our aim was to investigate the DET of different *Bm*F_{ald}DH fusion proteins between cyt b_{562} and the dehydrogenase. To achieve this, we designed various fusion protein constructs consisting of an N-terminal cyt b_{562} domain lacking the signal peptide for periplasmic export. These constructs contained either rigid, helical linker peptides that are aromatic rich [31], or flexible, non-conductive linker peptides [32] between the cyt b_{562} and the *Bm*F_{ald}DH. The aromatic-rich linker incorporates phenylalanine residues (L1) and the flexible linker (L2) is based on repeated $(GGGGS)_n$ motives (Fig. 2). We use cyclic

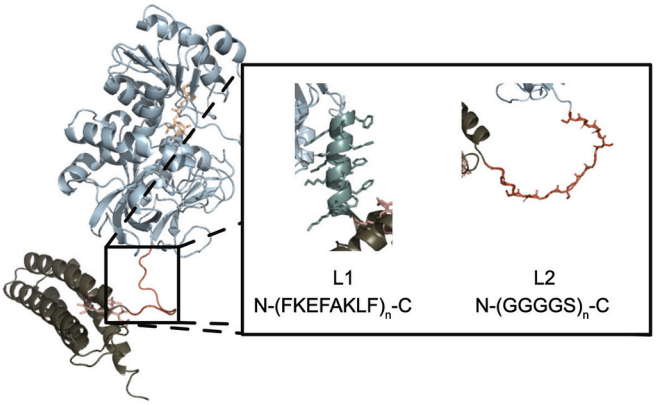

Fig. 2. Structural inside into the different linkers spaced between the N-terminus of the *Bm*F_{ald}DH and C-terminus of cyt b_{562}: Linker L1 refers to a phenylalanine rich alpha-helical linker and linker L2 is a glycine rich, flexible linker. Both are used in different lengths/ repetitions of the underlying amino acid motif (n = 1–4).

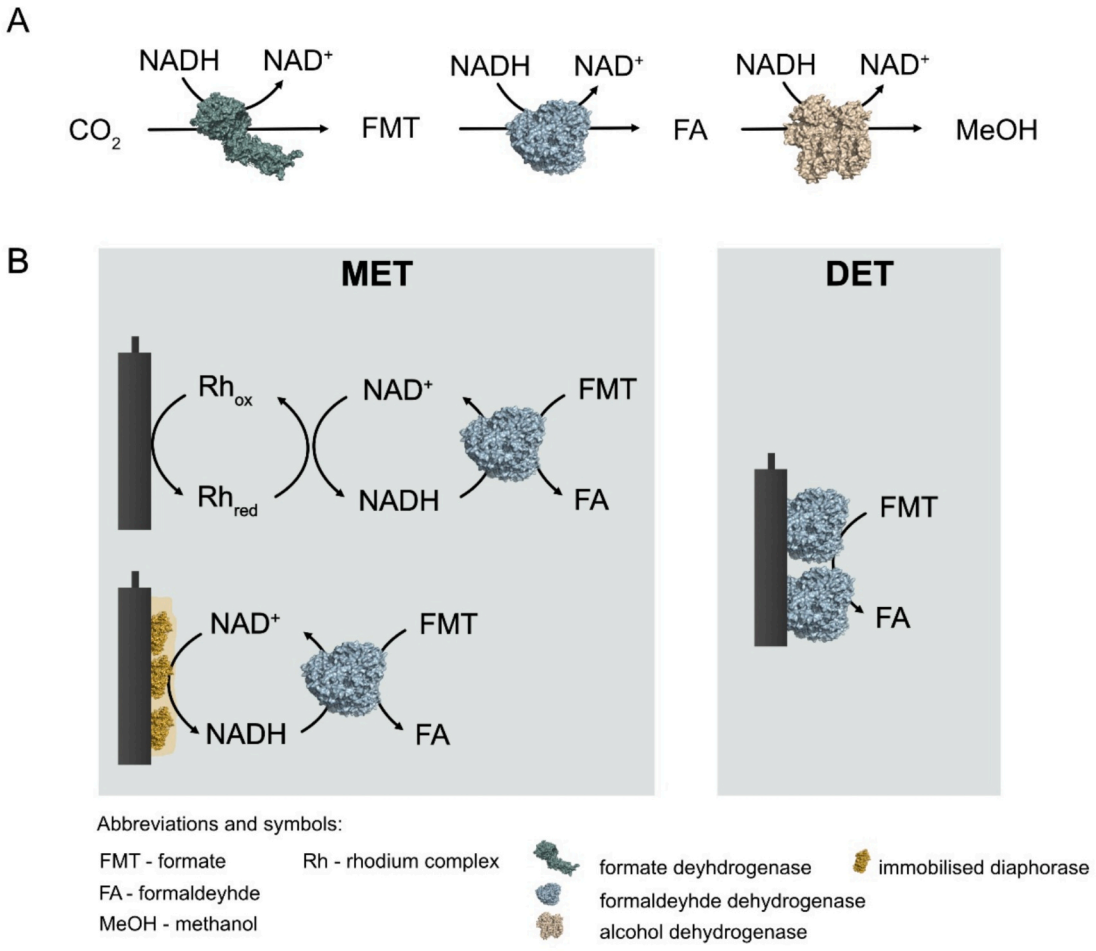

Fig. 1. Schematic overview of the enzymatic reduction of CO_2 to methanol. (**A**) Enzymatic cascade made of formate dehydrogenase (FDH), formaldehyde dehydrogenase (F_{ald}DH) and alcohol dehydrogenase (ADH). (**B**) Comparison of electron transfer pathways in the context of NADH regeneration (MET) and cofactor-free synthesis (DET).

voltammetry (CV) measurements to investigate and characterise the DET behaviour of the different fusion proteins to better understand and improve the DET behaviour of *Bm*F_{ald}DH. The main aim is to characterise and improve our understanding of the different fusion proteins by demonstrating a proof-of-concept reaction: the oxidation of FA to FMT in a biosensor application.

2. Material and methods

2.1. Chemicals, hardware and software

Chemicals were purchased from Carl Roth and Sigma-Aldrich. Photometric enzyme assays were conducted with an Agilent Cary 60 UV–Vis photometer and all electrochemical measurements were performed with a Gamry 1010 B and IMX B Multiplexer with the Gamry Instruments Framework software. Modelling of the enzymes, linkers and fusion proteins was performed with AlphaFold2 (Google DeepMind™) [33] and visualised using PyMOL (Schrödinger, LLC) [34]. SASA calculations were performed and visualised using PyMOL (Schrödinger, LLC) [34].

2.2. Protein expression, purification and enzyme assays

In this work fusion proteins between the formaldehyde dehydrogenase (*B. multivorans*, Uniprot J4QK49) and the soluble cyt b_{562} (*E. coli*, Uniprot P0ABE7) were constructed. The gene for the *Bm*F_{ald}DH was ordered from Twist Biosciences, the soluble cyt b_{562} was obtained through colony PCR from *E. coli* DH5α. Two different linker morphologies, a helical linker [31] and a flexible linker [32] were compared to each other. The helical linker was initially designed on the basis of *Geobacter sulfurreducens* nanowires and showed a conductive behaviour in self-assembled monolayers [31]. Linker sequences were codon-optimised (IDT) before insertion into the plasmid vector using Gibson cloning. For purification all constructs included a N-terminal His6-tag (Table SI 1). All plasmids were sequenced before further experiments (Microsynth). For the *Bm*F_{ald}DH, a 20 ml lysogenic broth (LB) preculture (shaking flask with baffles) grown overnight at 180 rpm and 37 °C was used to inoculate two 500 ml LB main cultures (shaking flask with baffles), which were induced with 0.1 mM IPTG at OD 0.4. Induced cultures were grown for 20 h at 20 °C with shaking at 130 rpm. For the cyt b_{562} fusion proteins and cyt b_{562}, a 20 ml LB preculture (shaking flask with baffles) grown overnight at 180 rpm and 37 °C was used to inoculate two 500 ml LB main cultures (shaking flasks without baffles), which were induced with 0.1 mM IPTG at OD 0.4. These cultures were grown at 16 °C and 100 rpm for 20 h, due to the oxygen sensitivity of the cyt b_{562} protein [30,35]. Cells were harvested through centrifugation (4000 ×*g*, 4 °C, 10 min) and stored at −20 °C for further use. For cell lysis, frozen cell pellets were thawed and resuspended in 15 ml lysis buffer (50 mM NaH_2PO_4, 300 mM NaCl, 10 mM imidazole, pH 7.5), DNAse I (Sigma-Aldrich), lysozyme (Sigma-Aldrich) and a protease inhibitor tablet (cOmplete™ EDTA-free, Roche) were added and the suspensions incubated in an orbital mixer for 60 min at 10 °C. Mechanical lysis was performed with sonication. Lysates were centrifuged (20.000 ×*g*, 4 °C, 60 min) and the supernatant filtered (0.45 μm) before performing IMAC purification (HisTrap™HP 1 ml, Cytiva). Following IMAC purification, a buffer exchange (50 mM NaH_2PO_4, 300 mM NaCl, pH 7.5) was performed with a desalting column (HiTrap™ desalting, 2 × 5 ml, Cytiva), the final fractions combined and stored in 20% glycerol at −80 °C for subsequent experiments. Protein quantification was performed using Bradford assay with a BSA calibration curve and SDS-PAGE analysis using Mini-Protean TGX Stain-Free Gels (4–20% gradient). SDS-PAGE gels were analysed using ImageJ software. Enzymatic activity assays were performed with 5 mM FA, 0.2 mM NAD^+ and adjustable volumes of the enzyme samples. The absorbance at 340 nm was measured for 4 min to indicate generation of NADH, due to the oxidation of FA to FMT. K_m and V_{max} values were obtained by varying the FA concentrations (0 mM, 0.005 mM, 0.01 mM, 0.05 mM, 0.1 mM, 2 mM, and 5 mM) with a set NAD^+ concentration of 0.2 mM and an enzyme amount of 0.33 nmol in 1 ml total volume. All initial reaction rates were determined with a python script, automatically assigning the highest number of possible data points to achieve a linear curve, aiming at highest R [2].

2.3. Electrode preparation and electro-enzymatic measurements

Gold electrodes (0.02 mm^2) were purchased from Pine Research and polished with fine grit paper before each experiment. Enzyme immobilisation was performed according to Teišerskytė et al. [7] All electrodes were incubated in phosphate buffer (100 mM, pH 7.0) for 10 min prior to the CV measurements to wash out non-bound protein. Bradford assay was performed to measure the amount of non-bound protein. CV measurement were conducted in 10 ml phosphate buffer with varying FA concentrations in a 3-electrode set up. Platinum wire was used as the counter electrode and an Ag/AgCl reference electrode (Pine Research) was used as a reference electrode. Measurements were performed with a sweep rate of 10 mV/s and step size of 5 mV in surface sampling mode. No additional cofactor was added to the electrochemical cells, to achieve cofactor free oxidation of FA. CV measurements were performed in N_2-gased puffer, to ensure an oxygen-free environment.

3. Results and discussion

3.1. Expression, purification and biochemical characterisation

Fusion proteins expressed within this study were modelled using AlphaFold2 prior to the experimental studies, to identify possible interfering structures and determine suitable linker lengths (Figure SI 1). All gene fragments encoding for cyt b_{562}, linker peptides and *Bm*F_{ald}DH were assembled into pET28(a) expression vector and expressed in *E. coli* BL21 DE3. For the rigid, helical linker (L1) three different lengths and for the flexible linker (L2) four different lengths were tested (Table 1). Additionally, one enzyme variant lacking a linker sequence was cloned and produced, to evaluate the initial need for a linker sequence.

The fusion proteins were isolated from the soluble protein fraction after cell disruption using IMAC and all final fractions exhibited a red colour, indicating the existence of heme, except for variant L1–21 (Figure SI 2). SDS-PAGE confirmed the presence of all fusion proteins at their expected sizes, except for L1–21 (Figure SI 3). After yielding again no protein after second expression of L1–21, we concluded that the long rigid linker interfered with proper protein folding and prevents successful recombinant expression. To identify active fusion proteins, oxidative activity assays using the purified protein were performed (Fig. 3). All enzyme variants exhibited oxidation activity towards FA, in addition a general trend towards higher specific activities was observed with the flexible linkers. The highest specific activity of an enzyme variant with a flexible linker was detected for L2–15, exhibiting 88% of the spec. Activity of the *Bm*F_{ald}DH. Lowest specific activities were employed for both linkers with the shorter sequences or the variant lacking a linker sequence. These results indicate that fusion proteins with both linker morphologies are recombinantly produced as soluble

Table 1
List of the *Bm*F_{ald}DH variants recombinantly produced in this work.

Enzyme variant	Linker type	Amino acid sequence linker N-C
L1–11	Rigid, helical, aromatic-rich	FKEFAKLFKEF
L1–15	Rigid, helical, aromatic-rich	FKEFAKLFKEFAKLF
L1–21	Rigid, helical, aromatic-rich	FKEFAKLFKEFAKLFHEFAKL
L2–5	Flexible, non-conductive	GGGGS
L2–10	Flexible, non-conductive	GGGGSGGGGS
L2–15	Flexible, non-conductive	GGGGSGGGGSGGGGS
L2–20	Flexible, non-conductive	GGGGSGGGGSGGGGSGGGGS
wo linker	No linker	–

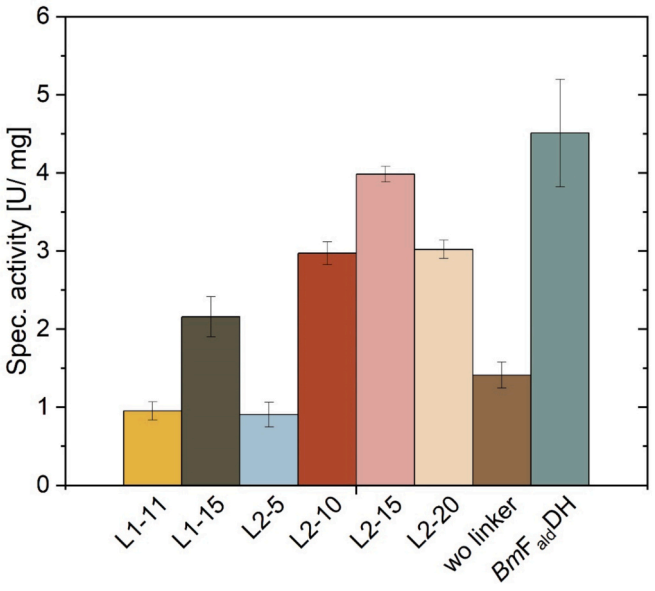

Fig. 3. Biochemical characterisation of *Bm*F_{ald}DH and enzyme variants. Specific activity [U/mg] of the final fractions obtained after purification. Variants: L1–11 (yellow), L1–15 (olive), L2–5 (light blue), L2–10 (red), L2–15 (pink), L2–20 (sand), wo linker (brown), and *Bm*F_{ald}DH (turquoise). Error bars represent the standard deviation from triplicate measurements. (For interpretation of the references to colour in this figure legend, the reader is referred to the web version of this article.)

proteins in *E. coli* BL21 and the catalytic activity of *Bm*F_{ald}DH was preserved with b_{562} fused at the N-terminus.

Further photometric analysis of all the enzyme variants was performed to identify the K_m, V_{max} and catalytic efficiency values (Table 2). The fusion proteins exhibited K_m values comparable to those of *Bm*F_{ald}DH; however, enzyme variants exhibiting L2 again had lower K_m values. These results are consistent with the specific activity data, in which L2 exhibited higher values than L1. Taking together, we hypothesise that linker L2 does not interfere with the structure of *Bm*F_{ald}DH, resulting in comparable specific activities and unaffected substrate affinity for variants with a linker longer than 10 amino acids.

3.2. Electrochemical characterisation

Electrodes were prepared according to the protocol described by Teišerskytė et al. and a non-coated electrode was used as a negative control during all experiments [7,25]. We started with immobilising the *Bm*F_{ald}DH on the gold electrode, to understand the DET behaviour of the wild-type enzyme. CV analysis was carried out in a potential range from −200 mV to +400 mV *vs.* Ag/AgCl with and without 20 mM FA (Fig. 4). Similar to already published results [7,36], we could detect a higher anodic current density with the enzyme coated electrode under the addition of FA to the electrochemical cell. The control electrode did not show any increase in anodic current after the addition of FA in the potential range from 0 mV to +250 mV *vs.* Ag/AgCl. Just as the potential was higher than +250 mV, the current began to rise, which indicates nonspecific oxidation of formaldehyde on the electrodes surface, which is known to occur at pH 7, but is more pronounced at alkaline conditions [7,37]. A similar behaviour was already shown by Teišerskytė and coworkers with *Pp*F_{ald}DH coated gold electrodes. These experiments clearly indicate, that the increase in anodic current density is enzyme related. Since no additional cofactor is added to the experiment solution, we propose, that the increase in anodic current density is due to DET related oxidation of FA.

To characterise DET for each of the fusion proteins and cyt b_{562}, we performed CV measurements with rising FA concentrations in the phosphate buffer. For each FA concentration the Δ current density was calculated by subtracting the current density at +400 mV *vs.* Ag/AgCl and 0 mM FA from the current density at +400 mV *vs.* Ag/AgCl with the corresponding FA concentration (Fig. 5). Results excluding unspecific FA oxidation, hence the current density at +200 mV *vs.* Ag/AgCl are shown in the supplementary information (Figure SI 4). The results at +200 mV *vs.* Ag/AgCl are comparable to those at +400 mV *vs.* Ag/AgCl and show an identical behaviour, however the differences are more pronounced at +400 mV *vs.* Ag/AgCl. An increase in anodic current in the potential range from +100 mV to +400 mV *vs.* Ag/AgCl, indicating FA oxidation activity, was detected for all fusion proteins (Figure SI 5–8). Most fusion proteins displayed current density values comparable to *Bm*F_{ald}DH. An exception to this trend was observable for the L2–20 variant, which exhibited a 1.5-fold increase in current density at +400 mV *vs.* Ag/AgCl. In the base line corrected Δ current density plot this increase is confirmed. Compared to *Pp*F_{ald}DH, variant L2–20 shows a 6.7-fold increase in current density at +200 mV *vs.* Ag/AgCl with 10 mM FA [7]. In the full potential range from −200 mV to +400 mV *vs.* Ag/AgCl no cytochrome specific peaks in current density were detected for the fusion proteins and the cyt b_{562} variant compared to the *Bm*F_{ald}DH. We hypothesise, that the cytochrome works as an electron relay and if active in the electron transfer, transfers them from the electrode to the active site of the enzyme.

Within tested FA concentration range, all tested enzyme variants exhibited a linear response in measured current density, despite their K_m values being in the range of 10–20 μM. Therefore, the enzymes were not substrate-inhibited when immobilised on Au-modified gold electrodes. This difference in K_m values can be explained by the structural stabilisation of the enzyme among the immobilisation and mass transfer limitations of the substrate, a phenomenon observed in other studies involving immobilised *Pp*F_{ald}DH [7] and alcohol dehydrogenase [38]. Variant L2–15, which exhibited the highest measurable specific activity during the biochemical characterisation, performed worse than *Bm*F_{ald}DH in the cofactor-free electrochemical tests. Additionally, variant L2–20, which exhibited lower specific activities than the other variants displayed significantly higher current densities at higher FA concentrations (Fig. 5c). The nonlinear correlation between the catalytic activity of the freely diffused enzyme and the current density in the CV measurements is presumably caused by the linker length. It is hypothesised that a linker of more than 15 amino acids interferes with the NAD^+/NADH access channel, when the enzyme is freely diffing in the reaction buffer, since K_m for FMT is identical for both enzyme variants. Consequently, a lower specific activity is detected for variant L2–20, compared to L2–15. However, this behaviour changes, when the enzyme is immobilised. Here longer L2 morphologies lead to increased current densities. It is hypothesised that the 20 amino acid flexible linker offers the greatest flexibility, which is required for the substrate to have access to the immobilised enzyme. The 20 amino acid linker also supports DET by coordinating the enzyme and fusion protein in a favourable

Table 2
K_m values [μM], V_{max} values [μmol/min] and catalytic efficiency [1/M*s] for fusion proteins and the *Bm*F_{ald}DH. The values were obtained from an oxidative enzymatic assay using FA as substrate at concentrations of 0 mM, 0.005 mM, 0.01 mM, 0.05 mM, 0.1 mM, 2 mM, 5 mM, and evaluated using Lineweaver-Burk regression. Errors were calculated *via* Gaussian error propagation and are reported as standard error.

Enzyme variant	$K_{m\ FA}$ [μM]	$V_{max\ FA}$ [μmol/min]	Catalytic efficiency [1/M*s]
L1–11	19 ± 7	13 ± 5	(37 ± 19) x 10^6
L1–15	19 ± 2	18 ± 2	(47 ± 7) x 10^6
L2–5	15 ± 2	8 ± 1	(37 ± 5) x 10^6
L2–10	11 ± 1	10 ± 1	(49 ± 7) x 10^6
L2–15	11 ± 1	16 ± 1	(73 ± 7) x 10^6
L2–20	11 ± 2	18 ± 3	(87 ± 18) x 10^6
wo linker	16 ± 1	16 ± 1	(49 ± 4) x 10^6
BmF_{ald}DH	12 ± 4	30 ± 9	(75 ± 23) x 10^6

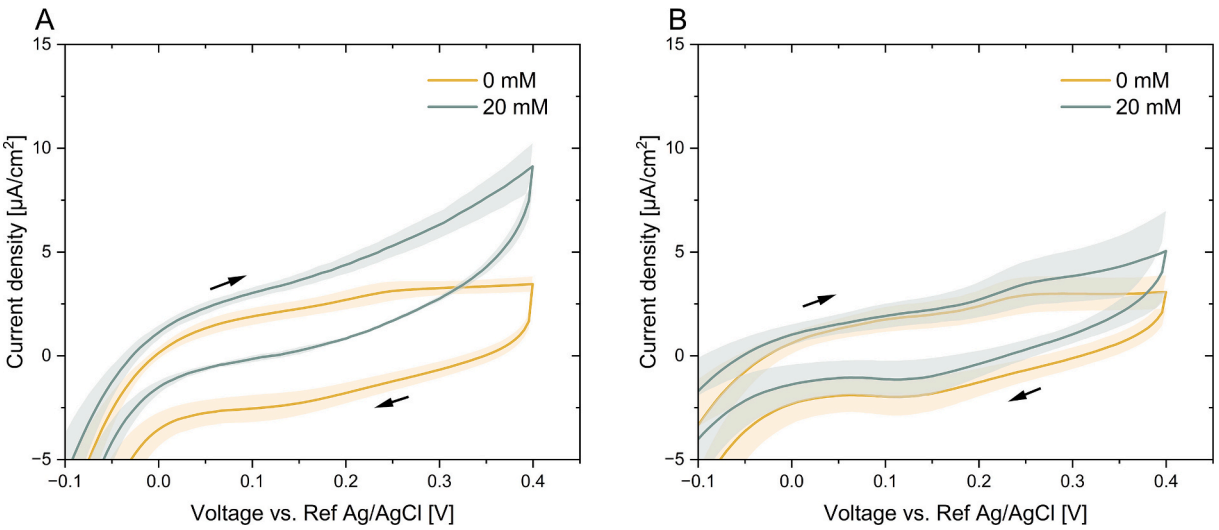

Fig. 4. CV measurements of the *Bm*F$_{ald}$DH coated gold electrode (**A**) and non-coated electrode (**B**) performed in a 3-electrode setup in a 10 ml undivided bio-electrochemical cell in 10 ml 100 mM phosphate buffer pH 7.0 (yellow) and with the addition of 20 mM FA (turquoise). Error bars represent the standard deviation from triplicate measurements. (For interpretation of the references to colour in this figure legend, the reader is referred to the web version of this article.)

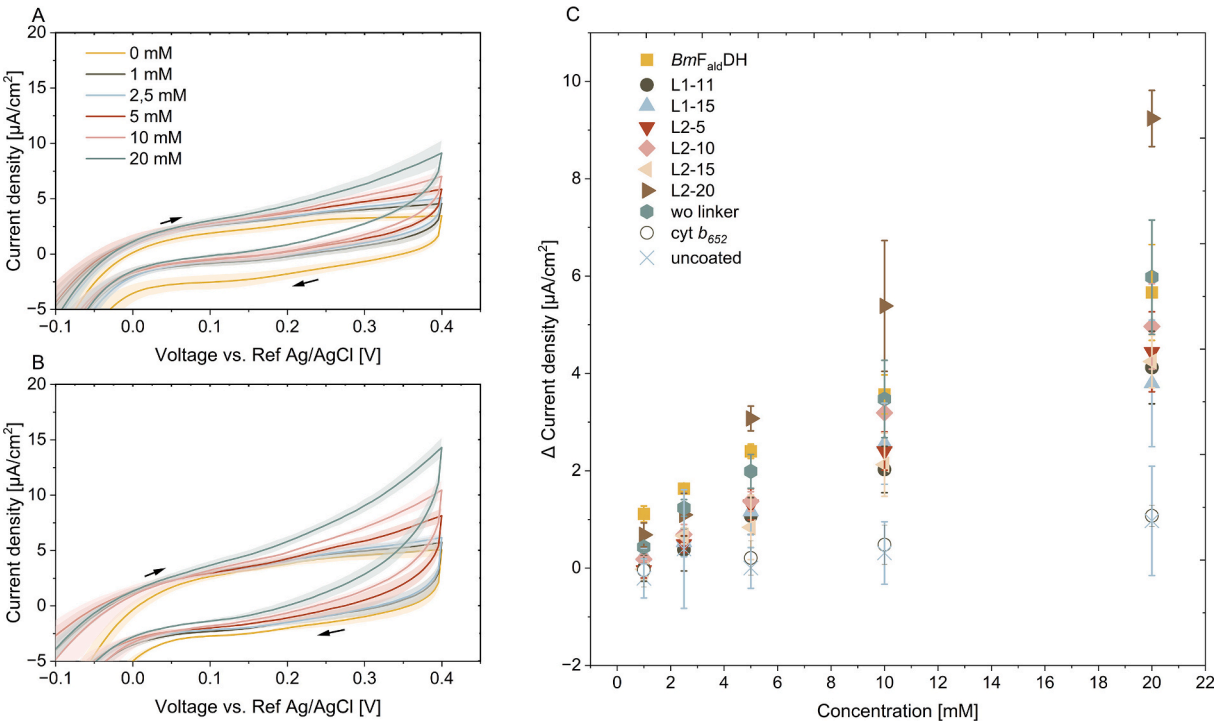

Fig. 5. Electrochemical characterisation of *Bm*F$_{ald}$DH and the fusion proteins. Cyclic voltammograms displayed as average current densities [µA/cm^2] plotted against voltage *vs.* Ag/AgCl reference electrode [V] for selected enzyme variants at varying FA concentrations: 0 mM (yellow), 1 mM (olive), 2.5 mM (light blue), 5 mM (red), 10 mM (pink), and 20 mM (turquoise). (**A**) *Bm*F$_{ald}$DH (**B**) L2–20. (**C**) Average baseline-corrected maximal current densities [µA/cm^2] at +400 mV, normalised to the corresponding buffer signal of each coated electrode (Δ current density). Measurements were performed at FA concentrations: 1 mM, 2.5 mM, 5 mM, 10 mM, and 20 mM. Symbols indicate the tested constructs: *Bm*F$_{ald}$DH (yellow square), L1–11 (olive circle), L1–15 (light blue triangle), L2–5 (red triangle), L2–10 (pink square), L2–15 (sand triangle), L2–20 (brown triangle), wo linker (turquois hexagon), cyt b_{562} (unfilled olive circle) and uncoated control (turquois X). (For interpretation of the references to colour in this figure legend, the reader is referred to the web version of this article.)

orientation on the electrode. In the example shown, linker lengths of less than 20 amino acids impede DET, as they do not offer the necessary flexibility to enable the enzyme variant to be oriented favourably on the electrode. All enzyme variants incorporating the helical L1 linker exhibited reduced DET capabilities compared to *Bm*F$_{ald}$DH and the L2 variants. This suggests that L1 does not facilitate electron hopping, either because it exists as a monomer and does not form a self-assembled monolayer, or because of its rigid morphology. In both cases, electron transfer between the heme of cyt b_{562} and the active site of the enzyme is impeded, presumably due to an increased distance between electron relays [39].

We calculated immobilisation efficiencies for each electrode and summarised the amount of bound protein as well as the surface coverage on each electrode (Table SI 2). For further evaluation of the enzyme

related catalytic activity, the current density of each individual electrode was normalised to the immobilised protein amount determined for each electrode (Figure SI 9). Three fusion proteins (L2–15, L2–20 and wo linker) exhibited higher enzymatic current densities than the *Bm*F_{ald}DH, with an increase of 2.5-fold for L2–15 and the wo linker variant.

3.3. The role of basic amino acids in the electrochemical characterisation of *Bm*F_{ald}DH

In addition, we performed further tests using immobilised bovine serum albumin (BSA) on gold electrodes to prove that the electrochemical current is caused by the catalytic activity of *Bm*F_{ald}DH (Fig. 6, Figure SI 8).

Unexpectedly we saw, that BSA exhibits an identical behaviour, an increase in current density at rising FA concentrations in the potential of +400 mV *vs.* Ag/AgCl. The same behaviour is observed at +200 mV *vs.* Ag/AgCl (Figure SI 10). To our knowledge there is no known catalytic activity of BSA towards FA [40]. After ruling out an insufficient cleaning of the electrode (data not shown), we expected a chemical reaction between the protein and FA to be the cause for the current response. The amino acids composition of BSA differs notably from *Bm*F_{ald}DH and the fusion proteins (Table SI 3–5). Basic amino acids like lysine, histidine and arginine are more abundant in BSA (23%) compared to the other proteins (*Bm*F_{ald}DH 18%, L2–20 17%). These amino acids are known to react with FA in a nucleophilic addition reaction that can form an imine, also known as a Schiff base, by cross-linking with other residues. (Fig. 7) [41–43]. This reaction is more profound under acidic conditions, but can to some extend happen at neutral pH. Also at pH 7.0, BSA adopts the N-form configuration, a structurally more relaxed form, which could promote protein cross-linking [43].

This effect could also occur in the enzymes variants, but likely to a lesser extent due to their tightly folded structure, which may result in a more shielded character, potentially caused by their tetrameric assembly state [45]. Moreover, BSA is known to adsorb onto Au surfaces *via* surface exposed cysteine and histidine residues [46]. This adsorption is further facilitated by the protein's loose tertiary structure, which improves the accessibility of these residues and might enable immobilisation despite electrostatic repulsion [46]. Given the results obtained

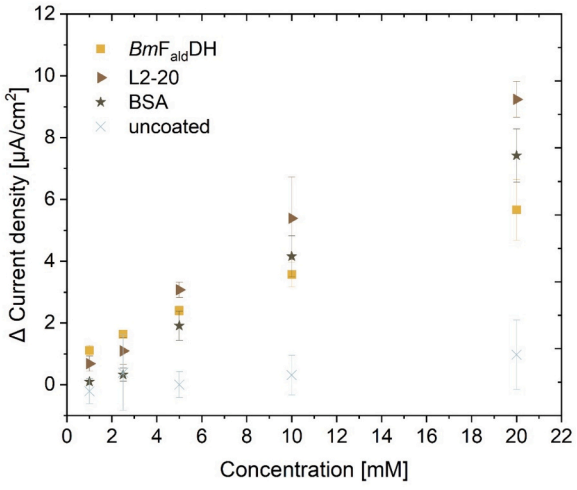

Fig. 6. Electrochemical characterisation of immobilised BSA compared to *Bm*F_{ald}DH and variant L2–20. Average baseline-corrected maximal current densities [μA/cm²] at +400 mV *vs.* Ag/AgCl, normalised to the corresponding buffer signal of each coated electrode (Δ current density). Measurements were performed at formaldehyde concentrations: 1 mM, 2.5 mM, 5 mM, 10 mM, and 20 mM. Symbols indicate the tested constructs: *Bm*F_{ald}DH (yellow square), L2–20 (brown triangle), BSA (olive star) and uncoated control (turquois X). (For interpretation of the references to colour in this figure legend, the reader is referred to the web version of this article.)

with BSA, we normalised the current and enzymatic current densities according to the percentage of basic amino acids present on the solvent-accessible surface area (SASA) of each enzyme variant (Fig. 8, Fig. 9). First, we calculated the number of basic amino acids on the surface area of each protein variant, then divided this number by the total number of amino acids on the protein's surface (Table SI 6).

This method allows the protein cross-link-associated currents to be neglected, hence a better distinction between oxidation dependent and side-reaction dependent currents is performed. Oxidation dependent currents are clearly visible for *Bm*F_{ald}DH and variant L2–20 at low FA concentrations (1–5 mM). Variant L2–20 exhibits a 1.6-fold improvement compared to *Bm*F_{ald}DH at the highest tested FA concentration at +400 mV *vs.* Ag/AgCl.

The interaction between basic amino acids and FA is an underexplored area in the field of biocatalytic CO_2 to methanol reduction. Only a few references have emerged, primarily in the context of biosensor development [41,42]. Although the reactivity of FA with these amino acids is well understood in the context of protein cross-linking and fixation, its influence on electrochemical measurements has not been thoroughly investigated. In this study we investigated the effect of these side reactions on CV measurements, by immobilising a non-catalytically active BSA on gold electrodes and measuring current densities depending on rising FA concentrations. The results revealed significant interference from FA side reactions with basic amino acids, resulting in non-catalytic currents in CV measurements. We found that normalising current responses based on amino acid composition on the proteins surface was essential for making more accurate comparisons during CV measurements. However, the presented normalisation method is still simplistic. In order to better determine the impact of current formation caused by side reactions, the orientation of the enzymes among immobilisation must be determined. The coordination of the enzymes has a huge impact on the SASA and location of the basic amino acids. By modelling the immobilisation of the enzyme on the electrodes surface, the estimation can be even improved and the normalisation refined. This modelling approach can also help to better understand electron transfer pathways from the electrode to the active site of the enzyme [47].

The presented approach provides a clearer insight into oxidation-dependent currents rather than responses dominated by FA side reactions. This method was used to characterise the seven fusion proteins between *Bm*F_{ald}DH and cyt b_{562} for their electrochemical DET behaviour in the oxidation of FA. One enzyme variant (L2−20) exhibited increased current densities at a potential range from +100 − +400 mV *vs.* Ag/AgCl. We propose, that the increased DET ability is caused by the fusion of the DET-capable protein cyt b_{562} with the longer flexible linker, ensuring intramolecular electron transfer from the active site of *Bm*F_{ald}DH towards the electrode.

4. Conclusion

In this study, novel *Bm*F_{ald}DH fusion proteins were successfully produced and comprehensively biochemically and electrochemically characterised. We found, that the flexible linker had low impact on the spec. Activity as well as the catalytic constants. Furthermore, the normalised data clearly indicates significant improvements in DET capabilities compared to *Bm*F_{ald}DH. To our knowledge, this is the first report showcasing an improvement of this enzyme in the context of electrochemistry, laying the foundation for future optimisation and application in industrial biocatalysis, especially in the field of CO_2 reduction. The understanding of the underlying electron transfer mechanisms of F_{ald}DH in bio electrochemical systems is key to design more efficient CO_2 reduction processes. Further understanding can be achieved through molecular dynamics simulations, which can be used to modulate protein interfacial conformation and electron transfer pathways [47]. These simulations must take into account the physical and chemical properties of the fusion proteins, as well as their immobilisation and absorption on

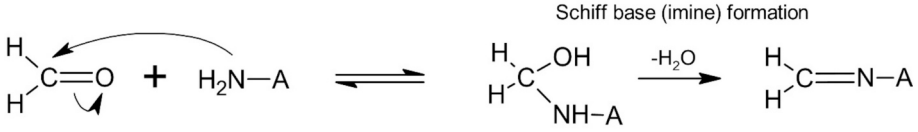

Fig. 7. Formaldehyde reaction with primary amines (*e.g.*, lysine) [44].

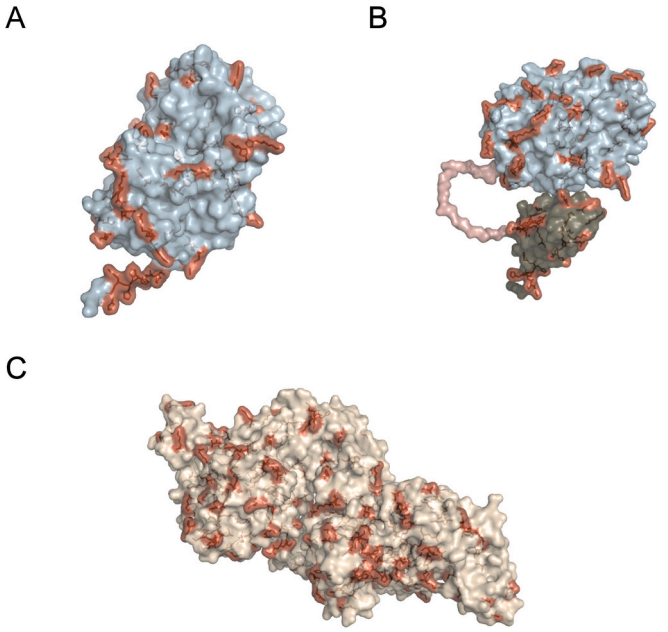

Fig. 8. SASA data for *Bm*F$_{ald}$DH (**A**), L2–20 (**B**) and BSA (**C**). SASA data was computed using PyMOL. Basic amino acids (Lys, Arg and His) are coloured in red. (For interpretation of the references to colour in this figure legend, the reader is referred to the web version of this article.)

an AU-coated gold electrode. Simulating the immobilisation of different fusion proteins on a gold electrode could provide a deeper understanding of how different linker morphologies influence DET. Furthermore, future research should focus on conducting chronoamperometric measurements to determine the FMT yield and verify the conversion of FA under cofactor-free conditions. This study has shown the necessity for running proper blind controls to understand, evaluate and improve electro-enzymatic systems.

Declaration of generative AI and AI-assisted technologies in the manuscript preparation process

During the preparation of this work the authors used DeepL Write and ChatGPT-4 in order to refine wording and grammar checking. After using these tools, the authors reviewed and edited the content as needed and take full responsibility for the content of the published article.

CRediT authorship contribution statement

Anna-Lena Drommershausen: Writing – original draft, Visualization, Validation, Methodology, Investigation, Formal analysis, Data curation, Conceptualization. **Bero H.G. Schnell:** Writing – review & editing, Methodology, Investigation. **Dirk Holtmann:** Writing – review & editing, Supervision, Resources, Project administration, Conceptualization.

Funding

The authors acknowledge the support and funding by the Federal Ministry of Research, Technology and Space (BMFTR, Germany, grant number 031B1398D).

Declaration of competing interest

The authors declare the following financial interests/personal relationships which may be considered as potential competing interests: Dirk Holtmann reports financial support was provided by Federal Ministry of Education and Research. If there are other authors, they declare that they have no known competing financial interests or personal

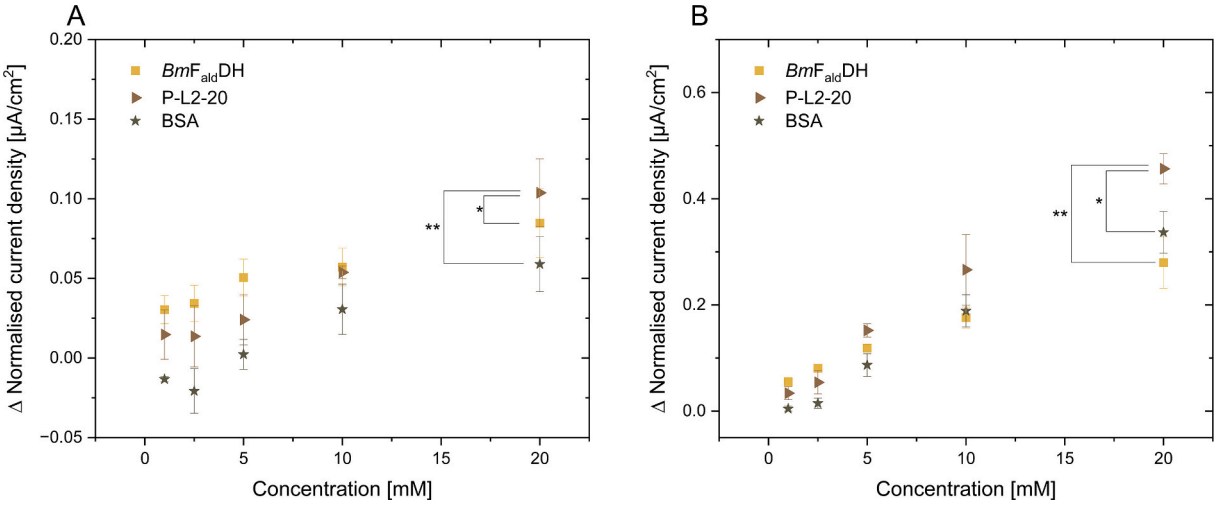

Fig. 9. Normalised current densities for *Bm*F$_{ald}$DH, variant L2–20 and BSA. Current densities are normalised to the percentage of basic amino acids present on the SASA of each protein variant. Measurements were performed at formaldehyde concentrations: 1 mM, 2.5 mM, 5 mM, 10 mM, and 20 mM at +200 mV *vs.* Ag/AgCl (**A**) and + 400 mV *vs.* Ag/AgCl (**B**). Symbols indicate the tested constructs: *Bm*F$_{ald}$DH (yellow square), L2–20 (brown triangle) and BSA (olive star). (For interpretation of the references to colour in this figure legend, the reader is referred to the web version of this article.)

relationships that could have appeared to influence the work reported in this paper.

Appendix A. Supplementary data

Supplementary data to this article can be found online at https://doi.org/10.1016/j.jelechem.2026.120044.

References

[1] Y. Liao, S. Chen, D. Wang, W. Zhang, S. Wang, J. Ding, Y. Wang, L. Cai, X. Ran, X. Wang, H. Zhu, Structure of formaldehyde dehydrogenase from *Pseudomonas aeruginosa*: the binary complex with the cofactor NAD^+, Acta Crystallographica Section F Structural Biology and Crystallization Communications 69 (2013) 967–972.

[2] N. Tanaka, Y. Kusakabe, K. Ito, T. Yoshimoto, K.T. Nakamura, Crystal structure of formaldehyde dehydrogenase from *pseudomonas putida*: the structural origin of the tightly bound cofactor in nicotinoprotein dehydrogenases, J. Mol. Biol. 324 (2002) 519–533.

[3] M. Ando, T. Yoshimoto, S. Ogushi, K. Rikitake, S. Shibata, D. Tsuru, Formaldehyde dehydrogenase from *Pseudomonas putida*, The Journal of Biochemistry 85 (1979) 1165–1172.

[4] Z.B. Rose, E. Racker, Formaldehyde dehydrogenase from bakers' yeast, J. Biol. Chem. 237 (1962) 3279–3281.

[5] P.C. Sanghani, C.L. Stone, B.D. Ray, E.V. Pindel, T.D. Hurley, W.F. Bosron, Kinetic mechanism of human glutathione-dependent formaldehyde dehydrogenase, Biochemistry 39 (2000) 10720–10729.

[6] G. Burgos-Barragan, N. Wit, J. Meiser, F.A. Dingler, M. Pietzke, L. Mulderrig, L. B. Pontel, I.V. Rosado, T.F. Brewer, R.L. Cordell, P.S. Monks, C.J. Chang, A. Vazquez, K.J. Patel, Mammals divert endogenous genotoxic formaldehyde into one-carbon metabolism, Nature 548 (2017) 549–554.

[7] V. Teišerskytė, J. Urbonavičius, D. Ratautas, A direct electron transfer formaldehyde dehydrogenase biosensor for the determination of formaldehyde in river water, Talanta 234 (2021) 122657.

[8] M. Aresta, A. Dibenedetto, C. Pastore, Biotechnology to develop innovative syntheses using CO_2, Environ. Chem. Lett. 3 (2005) 113–117.

[9] R. Obert, B.C. Dave, Enzymatic conversion of carbon dioxide to methanol: enhanced methanol production in silica sol−gel matrices, J. Am. Chem. Soc. 121 (1999) 12192–12193.

[10] S.-W. Xu, Y. Lu, J. Li, Z.-Y. Jiang, H. Wu, Efficient conversion of CO_2 to methanol catalysed by three dehydrogenases CO-encapsulated in an alginate−silica ($ALG-SiO_2$) hybrid gel, Ind. Eng. Chem. Res. 45 (2006) 4567–4573.

[11] R. Cazelles, J. Drone, F. Fajula, O. Ersen, S. Moldovan, A. Galarneau, Reduction of CO_2 to methanol by a polyenzymatic system encapsulated in phospholipids–silica nanocapsules, New J. Chem. 37 (2013) 3721.

[12] J. Luo, A.S. Meyer, R.V. Mateiu, M. Pinelo, Cascade catalysis in membranes with enzyme immobilization for multi-enzymatic conversion of CO_2 to methanol, N. Biotechnol. 32 (2015) 319–327.

[13] C. Di Spiridione, M. Aresta, A. Dibenedetto, Improving the enzymatic cascade of reactions for the reduction of CO_2 to CH_3OH in water: from enzymes immobilization strategies to cofactor regeneration and cofactor suppression, Molecules 27 (2022) 4913.

[14] S.K. Kuk, R.K. Singh, D.H. Nam, R. Singh, J.-K. Lee, C.B. Park, Photoelectrochemical reduction of carbon dioxide to methanol through a highly efficient enzyme cascade, Angew. Chem. Int. Ed. 56 (2017) 3827–3832.

[15] S. Schlager, A. Dibenedetto, M. Aresta, D.H. Apaydin, L.M. Dumitru, H. Neugebauer, N.S. Sariciftci, Biocatalytic and bioelectrocatalytic approaches for the reduction of carbon dioxide using enzymes, Energ. Technol. 5 (2017) 812–821.

[16] S. Schlager, A. Fuchsbauer, M. Haberbauer, H. Neugebauer, N.S. Sariciftci, Carbon dioxide conversion to synthetic fuels using biocatalytic electrodes, J. Mater. Chem. A 5 (2017) 2429–2443.

[17] K. Sakai, Y. Kitazumi, O. Shirai, K. Takagi, K. Kano, Direct electron transfer-type four-way bioelectrocatalysis of CO_2/formate and NAD^+/NADH redox couples by tungsten-containing formate dehydrogenase adsorbed on gold nanoparticle-embedded mesoporous carbon electrodes modified with 4-mercaptopyridine, Electrochem. Commun. 84 (2017) 75–79.

[18] T. Reda, C.M. Plugge, N.J. Abram, J. Hirst, Reversible interconversion of carbon dioxide and formate by an electroactive enzyme, Proc. Natl. Acad. Sci. 105 (2008) 10654–10658.

[19] M.V. Bram, J. Liniger, S.S. Majidabad, H.R. Shabani, M.P.R. Teles, X. Cui, Challenges in power-to-X: a perspective of the configuration and control process for E-methanol production, Int. J. Hydrogen Energy 76 (2024) 315–325.

[20] P. Wang, X. Wang, S. Chandra, A. Lielpetere, T. Quast, F. Conzuelo, W. Schuhmann, Hybrid enzyme-electrocatalyst cascade modified gas-diffusion electrodes for methanol formation from carbon dioxide, Angew. Chem. Int. Ed. 64 (2025) e202422882.

[21] F. Hollmann, A. Schmid, Electrochemical regeneration of oxidoreductases for cell-free biocatalytic redox reactions, Biocatal. Biotransformation 22 (2004) 63–88.

[22] F. Lima, G. Maia, Direct electron transfer from alcohol dehydrogenase, RSC Adv. 4 (2014) 22575.

[23] R.K. Singh, R. Singh, D. Sivakumar, S. Kondaveeti, T. Kim, J. Li, B.H. Sung, B.-K. Cho, D.R. Kim, S.C. Kim, V.C. Kalia, Y.-H.P.J. Zhang, H. Zhao, Y.C. Kang, J.-K. Lee, Insights into cell-free conversion of CO_2 to chemicals by a multienzyme cascade reaction, ACS Catal. 8 (2018) 11085–11093.

[24] O. Smutok, T. Kavetskyy, E. Katz, "recent trends in enzyme engineering aiming to improve bioelectrocatalysis proceeding with direct electron transfer" *current opinion in*, Electrochemistry 31 (2022) 100856.

[25] I. Algov, L. Alfonta, Use of protein engineering to elucidate electron transfer pathways between proteins and electrodes, ACS Measurement Science Au 2 (2022) 78–90.

[26] Y. Kaida, Y. Hibino, Y. Kitazumi, O. Shirai, K. Kano, Ultimate downsizing of d-fructose dehydrogenase for improving the performance of direct electron transfer-type bioelectrocatalysis, Electrochem. Commun. 98 (2019) 101–105.

[27] Y. Kaida, Y. Hibino, Y. Kitazumi, O. Shirai, K. Kano, Discussion on direct electron transfer-type bioelectrocatalysis of downsized and axial-ligand exchanged variants of d-fructose dehydrogenase, Electrochemistry 88 (2020) 195–199.

[28] J.T. Holland, C. Lau, S. Brozik, P. Atanassov, S. Banta, Engineering of glucose oxidase for direct electron transfer via site-specific gold nanoparticle conjugation, J. Am. Chem. Soc. 133 (2011) 19262–19265.

[29] S. Zernia, R. Frank, R.H.J. Weiße, H.G. Jahnke, K. Bellmann-Sickert, A. Prager, B. Abel, N. Sträter, A. Robitzki, A.G. Beck-Sickinger, Surface-binding peptide facilitates electricity-driven NADPH-free cytochrome P450 catalysis, ChemCatChem 10 (2018) 525–530.

[30] T. Yanase, J. Okuda-Shimazaki, K. Mori, K. Kojima, W. Tsugawa, K. Sode, Creation of a novel DET type FAD glucose dehydrogenase harboring *Escherichia coli* derived cytochrome b_{562} as an electron transfer domain, Biochem. Biophys. Res. Commun. 530 (2020) 82–86.

[31] R.C.G. Creasey, A.B. Mostert, A. Solemanifar, T.A.H. Nguyen, B. Virdis, S. Freguia, B. Laycock, Biomimetic peptide nanowires designed for conductivity, ACS Omega 4 (2019) 1748–1756.

[32] X. Chen, J.L. Zaro, W.-C. Shen, Fusion protein linkers: property, design and functionality, Adv. Drug Deliv. Rev. 65 (2013) 1357–1369.

[33] J. Jumper, R. Evans, A. Pritzel, T. Green, M. Figurnov, O. Ronneberger, K. Tunyasuvunakool, R. Bates, A. Žídek, A. Potapenko, A. Bridgland, C. Meyer, S.A. A. Kohl, A.J. Ballard, A. Cowie, B. Romera-Paredes, S. Nikolov, R. Jain, J. Adler, T. Back, S. Petersen, D. Reiman, E. Clancy, M. Zielinski, M. Steinegger, M. Pacholska, T. Berghammer, S. Bodenstein, D. Silver, O. Vinyals, A.W. Senior, K. Kavukcuoglu, P. Kohli, D. Hassabis, Highly accurate protein structure prediction with AlphaFold, Nature 596 (2021) 583–589.

[34] Schrodinger, LLC, 2015.

[35] H. Nikkila, R.B. Gennis, S.G. Sligar, Cloning and expression of the gene encoding the soluble cytochrome b_{562} of *Escherichia coli*, Eur. J. Biochem. 202 (1991) 309–313.

[36] Z.E. Shaked, J.J. Barber, G.M. Whitesides, Combined electrochemical/enzymic method for *in situ* regeneration of NADH based on cathodic reduction of cyclic disulfides, J. Org. Chem. 46 (1981) 4100–4101.

[37] M. BeŁtowska-Brzezinska, Electrochemical oxidation of formaldehyde on gold and silver, Electrochim. Acta 30 (1985) 1193–1198.

[38] S. Ghannadi, H. Abdizadeh, M. Miroliaei, A.A. Saboury, Immobilisation of alcohol dehydrogenase on titania nanoparticles to enhance enzyme stability and remove substrate inhibition in the reaction of formaldehyde to methanol, Industrial & Engineering Chemistry Research 58 (2019) 9844–9854.

[39] A. Le Goff, M. Holzinger, Molecular engineering of the bio/nano-interface for enzymatic electrocatalysis in fuel cells, Sustainable Energy & Fuels 2 (2018) 2555–2566.

[40] E.L. Borucki, L.E. Iglesias, Recent applications of albumin as a green and versatile catalyst in organic synthesis, Molecules 30 (2025) 4168.

[41] B. Metz, G.F.A. Kersten, P. Hoogerhout, H.F. Brugghe, H.A.M. Timmermans, A. De Jong, H. Meiring, J. Ten Hove, W.E. Hennink, D.J.A. Crommelin, W. Jiskoot, Identification of formaldehyde-induced modifications in proteins, J. Biol. Chem. 279 (2004) 6235–6243.

[42] T. Hutapea, M. Syaputra, F. Kurniawan, Green chemistry approach to formaldehyde detection using fish albumin-modified gold electrodes, Global Journal of Environmental Science and Management 11 (2025) 791–804.

[43] M. Zhang, H.J. Vogel, Determination of the side chain pKa values of the lysine residues in calmodulin, J. Biol. Chem. 268 (1993) 22420–22428.

[44] ChemSketch, version 2022.1.2 ed., Advanced Chemistry Development, Inc. (ACD/Labs), Toronto, ON, Canada. www.acdlabs.com, 2026.

[45] D.S. Goodsell, A.J. Olson, Structural symmetry and protein function, Annu. Rev. Biophys. 29 (2000) 105–153.

[46] D.-H. Tsai, F.W. Delrio, A.M. Keene, K.M. Tyner, R.I. Maccuspie, T.J. Cho, M. R. Zachariah, V.A. Hackley, Adsorption and conformation of serum albumin protein on gold nanoparticles investigated using dimensional measurements and *in situ* spectroscopic methods, Langmuir 27 (2011) 2464–2477.

[47] D. Zhao, L. Li, J. Zhou, Simulation insight into the cytochrome c adsorption on graphene and graphene oxide surfaces, Appl. Surf. Sci. 428 (2018) 825–834.